PERGAMON

International Journal of Solids and Structures 40 (2003) 5305–5318

INTERNATIONAL JOURNAL OF SOLIDS and STRUCTURES

www.elsevier.com/locate/ijsolstr

Lightning-induced fracture of masonry and rock

James F. Wilson *

Duke University, 6319 Mimosa, Dr. Chapel Hill, NC 27514, USA

Received 15 November 2002; received in revised form 20 April 2003

Abstract

As a lightning channel on its way to ground meets a standing masonry or rock structure, radiant energy from the channel can induce a thermal shock of sufficient intensity to cause the structure to fracture and collapse. Mathematical models for two such structural failure mechanisms are proposed: one describing violent surface separations or spalling, and the other characterizing internal cracking from sudden increased pore pressure in the solid. Experimental data and case studies are used to complement these theories of lightning-induced failure.
© 2003 Elsevier Ltd. All rights reserved.

Keywords: Concrete; Elasticity; Fracture; Lightning; Masonry; Stone; Thermal shock

1. Introduction

Using lightning rods (air terminals) in carefully placed positions on structures, the structures can be protected from the damage of most lightning strikes. For instance, Petrov and D'Alessandro (2002) analyzed lightning strike data obtained for 161 buildings in Hong Kong, data that spanned the period 1988–1996; but those structures escaped damage because they were protected with lightning rods positioned using a collection volume method described by D'Alessandro and Gumley (2001). For structures not so protected, lightning strikes damage or destroy more buildings than do other weather-related events, including tornadoes, hurricanes and floods. For instance, in a typical year in the United States, lightning burns or otherwise significantly damages about 30 000 unprotected buildings, of which about 18 000 are private homes (Frydenlund, 1986).

The main purpose of the present investigation is to introduce two new quantitative mathematical models for the lightning-induced failure of unprotected masonry and rock structures in the open air: explosive surface spalling and explosive internal crack propagation. The relevant measured properties of the type of lightning that can lead to these two types of structural failure have been summarized in the extensive works of Uman (1984) and Krider (1982). Such properties include the duration, geometry, and intensity of radiant energy associated with the stepped lightning leaders. That the two failure mechanisms can be brought about

* Address: Department of Civil and Environment Engineering, Duke University, P.O. Box 90287, Durham, NC 27708 0287, USA. Fax: +1-919-660-5219.

E-mail address: jwilson@duke.edu (J.F. Wilson).

0020-7683/$ - see front matter © 2003 Elsevier Ltd. All rights reserved.
doi:10.1016/S0020-7683(03)00289-0

by temperature gradients induced in solids was suggested by Bazant and Kaplan (1996), who discussed experiments on the fracture of concrete blocks subjected to slow heating (periods of hours). Related work includes that of Sadowsky (1955), who analyzed spalling caused by fast heating (periods of seconds) for a radiated circular disk on half-space; and the analyses by Wilson (1977, 2000) of lightning-induced, explosive internal crack propagation of partly buried cement block foundation walls. The two failure models herein, which involve lightning-induced thermal shock to solids, conduction heat transfer, classical elasticity, and fracture mechanics, are significant extensions of the Sadowsky and Wilson studies. It will be shown that spalling of masonry blocks and rocks can occur for temperatures suddenly elevated above 550 °C; and that internal explosive behavior, which is due to elevated pore water pressure in these solids, can occur for temperatures suddenly elevated to only 30 °C.

This paper begins with a very brief description of lightning, followed by a summary of data on the lightning channel that induces failure in masonry and rock structures, whether buried or in the open air. Heat transfer and thermal stress for each of the two failure models are then discussed. The paper concludes with two case studies: the splitting of a common concrete building block struck by laboratory sparks that simulate lightning strikes; and the toppling of a 4 m high sandstone monument struck by a lightning leader. This monument is one of the rocks erected about 2500 BC in the Ring of Brodgar, located in the Orkney Islands.

2. Physical properties of lightning flashes

Lightning has been defined as a transient, high-current discharge, most commonly produced in a thundercloud (cumulonimbus), which is nominally 5 km above the ground. Discharges of cloud-to-ground lightning is characterized by a channel of current flow propagating from cloud to ground, called the *stepped leader*. The usually observed stepped leader lowers the cloud's negative charge, has three or four high energy discharges called *negative strokes*, which together is designated as the *flash* of the stepped leader. Following the flash is the *return stroke*, a more luminous channel of current flow propagating back to its cloud of origin. Observed less frequently is the stepped leader that lowers the cloud's positive charge, which generally has a single *positive stroke* of higher current than that in the more frequently observed negative strokes. When striking a masonry or rock structure, either type of flash can radiate sufficient energy to damage the structure.

Summarized in Table 1 are some of the measured physical properties of the flashes associated with strepped lightning leaders. Each physical property (minimum, nominal, maximum) represents an *average* of observed values for the channel. In the present analysis, the *nominal* average properties are assumed to

Table 1
Selected properties measured for streaked lightning stepped leaders (Krider, 1982; Uman, 1984)

	Property	Minimum	Nominal	Maximum
c	Radius of channel core (cm)	1.5	6.6	11.5
c_0	Outer radius of plasma channel (m)	1	5	10
d	Path length, cloud base to ground (km)	2	5	14
f_r	Fraction of Q that is radiated	0.006	0.01	0.02
Δt	Duration of flash (s)	0.01	0.2–0.5	2–20
v	Plasma velocity (m/s)	0.8×10^5	2.0×10^5	2.4×10^6
I_0	Channel core current (A)	38	100	580
Q	Channel energy dissipated (total) (J/m)	–	1×10^5	2×10^5
T	Channel core temperature (°C)	1700	2700	3700
V_0	Channel voltage, cloud base to ground (V)	–	1×10^8	–

govern structural damage. The most uncertain data in Table 1 are those for the current-carrying core radius c. This core is difficult to measure photographically because it is obscured by a corona sheath, with a radius c_0 of 1–10 m, surrounding this core. However, the values of c reported in Table 1 are supported by calculations based on spectral measurements of Orville et al. (1967) as discussed by Uman (1984). Those values of c are also consistent with measurements of long sparks produced in the laboratory: channel sparks several meters long, with currents up to hundreds of amperes, and voltage potentials of about 10^6 V. The total energy per unit length that is dissipated by the plasma channel of a lightning leader as it travels from the cloud base to ground at the potential of 10^8 V is $Q = 10^5$ J/m. Spectral measurements indicate that a fraction f_r (approximately 1%) of this unit energy is dissipated as radiation.

3. Thermal shock and spalling

3.1. Thermal loading

The spalling model and its coordinate system are defined in Fig. 1. The vertical surface is a portion of a standing masonry wall or rock, treated as a linear elastic solid. A lightning leader has struck the top of this solid and its current-carrying channel core of radius c seeks ground as it radiates energy to the vertical surface of the solid. The solid strip of width $2c$ and thickness h is assumed to be the only portion of the solid that receives radiated energy from the channel core, which is tangent to the wall. Further assumptions for this model are that the strip is very thin ($h \ll 2c$) and that during the flash strike time Δt, the whole volume of the strip is at a uniform, mean temperature $\overline{T}$ above ambient, while the rest of the solid remains at ambient temperature for most of the duration Δt. Thus, during the strike, the thin strip remains fully confined long its edges $x = \pm c$, although free expansion is allowed for the strip on its face plane $y = 0$. The strip is thus in plane stress, or $\sigma_y = 0$. Further, for most of its vertical length, the strip is in plane strain ($\varepsilon_x = \varepsilon_z = 0$). The assumptions for this strip model are parallel to those for the two-dimensionally hydrostatic radiated circular disk model investigated by Sadowsky (1955).

Based on these assumptions, it follows from Timoshenko and Goodier (1951) that the strip's compressive normal stress acting at the edges of the strip, at $x = \pm c$, is given by

$$\sigma_0 = \frac{E\alpha_0\overline{T}}{1-\nu} \tag{1}$$

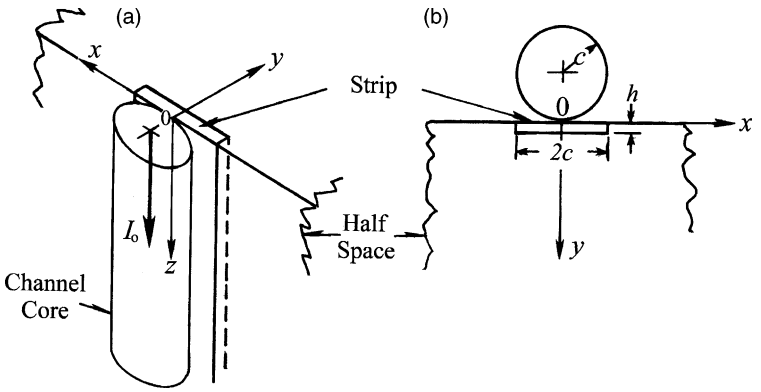

Fig. 1. The strip model for spalling showing: (a) a vertical section of the lightning channel core, which is tangent to the surface of half-space and (b) the cross-section for the plane $z = 0$.

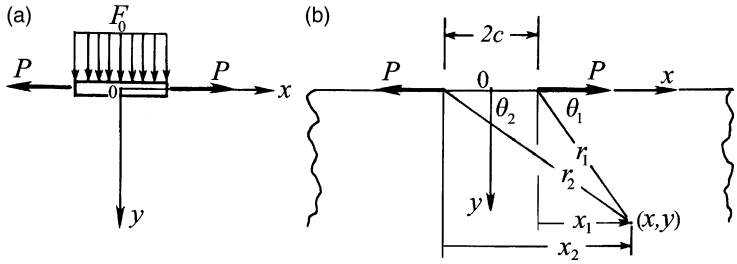

Fig. 2. Cross-sections of the spalling model showing: (a) thermal flux and edge load on the isolated, two-dimensional hydrostatic strip and (b) thermal loading of half-space.

in which E, v, and α_0 are Young's modulus, Poisson's ratio, and the coefficient of linear expansion of the solid, respectively. This compressive edge stress completely supresses the temperature-induced expansion of the strip width. The corresponding edge load P per unit length along z of the strip, illustrated in Fig. 2a, is thus

$$P = \sigma_0 h = \frac{E\alpha_0 \overline{T}}{1-v} h \tag{2}$$

The pair of equal and opposite reaction loads P on the surface of half-space are shown in Fig. 2b.

3.2. Heat flux

To compute $\overline{T}$, it is necessary to estimate the heat flux F_0, which acts on the strip during the flash time Δt. Define F_0, directed as shown in Fig. 2a, as the average radiated power per unit surface area of the strip. Let f_s be the fraction of the total radiated unit energy $f_r Q$ that is radiated directly to the strip; let d be the channel length from the cloud base to ground, and let v be the plasma velocity. In these terms, the first estimate of this flux is deduced as

$$F_0 = \frac{f_s f_r Q}{2c}\left(\frac{v}{d}\right) \tag{3}$$

With an assumed value of $f_s = 0.25$ and with the nominal values of the other parameters given in Table 1, Eq. (3) gives $F_0 = 83.3$ kW/m^2.

A second estimate of F_0 is

$$F_0 = \frac{f_s f_r V_0 I_0}{2cd} \tag{4}$$

in which V_0 is the average voltage potential between the cloud base and ground, and I_0 is the average channel current for the flash. Note that $V_0 I_0/d$ is the total available channel power per unit length, that $f_r V_0 I_0/d$ is the portion of that power that is dissipated in radiation, and that $f_s f_r V_0 I_0/(2cd)$ is the portion of the channel power per unit area that is radiated to the solid strip of width $2c$. For the lightning properties given in Table 1, the flux computed from Eq. (4) is $F_0 = 37.9$ kW/m^2.

Considering the fact that the data upon which the two estimates of F_0 are based depend on properties measured in different ways by different researchers for different lightning events, there is reasonable agreement between them. As a reference value in subsequent studies, an average value for the two estimates will be used, or $F_0 = 60.6$ kW/m^2.

3.3. Temperature distribution

For a short radiation time, it is reasonable to assume that the heat flow is mainly along the y-direction, with negligible dispersion along x. This assumption leads to an upper bound for the temperature change $T = T(y,t)$ on the plane $x = 0$, which can then be found by solving the following classical heat conduction equation.

$$\alpha \frac{\partial^2 T}{\partial y^2} = \frac{\partial T}{\partial t}; \quad \alpha = \frac{k}{\gamma c_p} \tag{5}$$

Here α is the thermal diffusivity and k is the thermal conductivity of the solid. The strip surface is subject to a constant heat flux, or

$$F_0 = -k \frac{\partial T}{\partial y}; \quad y = 0, \quad 0 \leqslant t \leqslant \Delta t \tag{6}$$

where Δt is the flash strike time. The classical solution to Eq. (5) with the boundary condition (6) is given by Carslaw and Jaegar (1990) as

$$T = \frac{2F_0}{k}\left[\left(\frac{\alpha t}{\pi}\right)^{1/2} \exp\left(\frac{-y^2}{4\alpha t}\right) - \frac{y}{2}\operatorname{erf}c\left(\frac{y}{2\sqrt{\alpha t}}\right)\right] \tag{7}$$

in which $\operatorname{erf}c$ is the complementary error function. Numerical results for temperature distributions will be presented as a part of the case studies.

3.4. Thermal stresses

The thermal shock load for spalling is now reduced to a problem in classical elasticity in which there are two loads per unit length P applied to half-space at the surface points $x = \pm c$, as shown in Fig. 2b. The corresponding stress field was originally derived by Michell (1900) and later discussed by Timoshenko and Goodier (1951). When the stresses for the two opposing loads P of Fig. 2b are superimposed, the results become

$$\sigma_x = \frac{2P}{\pi}\left[-\frac{\cos^4\theta_1}{x_1} + \frac{\cos^4\theta_2}{x_2}\right] \tag{8}$$

$$\sigma_y = \frac{2P}{\pi}\left[-\frac{\sin^2\theta_1\cos^2\theta_1}{x_1} + \frac{\sin^2\theta_2\cos\theta_2}{x_2}\right] \tag{9}$$

$$\tau_{xy} = \frac{2P}{\pi}\left[-\frac{\sin\theta_1\cos^3\theta_1}{x_1} + \frac{\sin\theta_2\cos^3\theta_2}{x_2}\right] \tag{10}$$

$$\sigma_z = v(\sigma_x + \sigma_y) \tag{11}$$

The stress σ_z is based on the plane strain assumption, $\varepsilon_z = 0$. Even though these stresses are singular at the points of load application, these solutions are satisfactory in the present problem in which the stresses are sought along the plane of symmetry, $x = 0$.

This system can be cast in nondimensional form as follows. Define the nondimensional coordinates based on the Cartesian system of Fig. 2 as

$$\bar{x} = x/c; \quad \bar{y} = y/c; \quad \bar{z} = z/c \tag{12}$$

In these terms, Eqs. (8)–(11) can be written in nondimensional form as

$$\frac{\sigma_x}{R} = D_1(\bar{x}+1)^3 - D_2(\bar{x}-1)^3 \tag{13}$$

$$\frac{\sigma_y}{R} = D_1\bar{y}^2(\bar{x}+1) - D_2\bar{y}^2(\bar{x}-1) \tag{14}$$

$$\frac{\tau_{xy}}{R} = D_1\bar{y}(\bar{x}+1)^2 - D_2\bar{y}(\bar{x}-1)^2 \tag{15}$$

$$\frac{\sigma_z}{R} = v(\bar{\sigma}_x + \bar{\sigma}_y) \tag{16}$$

In Eqs. (13)–(16), $R = 2P/(\pi c)$, and is defined as the radiant heat parameter and has units of stress. Using Eq. (2), this parameter can be expressed in terms of the mean strip temperature, or

$$R = \frac{2P}{\pi c} = \frac{2E\alpha_0\overline{T}}{\pi c(1-v)}h \tag{17}$$

In Eqs. (13)–(16), the coordinate parameters D_1 and D_2 are defined as

$$D_1 = [\bar{y}^2 + (\bar{x}+1)^2]^{-2}; \quad D_2 = [\bar{y}^2 + (\bar{x}-1)^2]^{-2} \tag{18}$$

Thus, by specifying the coordinate point (x, y), the strip half width c, and the radiant heat parameter R, the coordinate parameters can be calculated from Eqs. (12) and (18), and the corresponding stresses can be computed from Eqs. (13)–(16).

Of particular interest are the stress distributions as a function of depth y, and along the plane of potential fracture, $x = 0$. On this plane, the shear stress τ_{xy} is zero for all y, as it should be, since the two horizontal loads P are symmetrically placed with respect to the plane $x = 0$. Shown in Fig. 3 are plots of the stresses as a function of the depth y/c, computed from Eqs. (13), (14) and (16) on the plane $x = 0$. Of interest in the present problem are the peak stresses, which are $\sigma_x = 2R$, $\sigma_y = 0.4R$, and $\sigma_z = 0.5R$. The peak stresses σ_x and σ_z occur just under the strip thickness h (or at $y = 0$ for all practical purposes), and the peak stress σ_y is beneath the surface, at $y = c$.

With these results, the critical mean temperature $\overline{T} = \overline{T}_t$ required for spalling can be computed. That is, let $\sigma_x = 2R = \sigma_t$ where σ_t is the tensile strength of the solid. It follows from Eq. (17) that

$$\overline{T}_t = \frac{\pi c(1-v)\sigma_t}{4E\alpha_0 h} \tag{19}$$

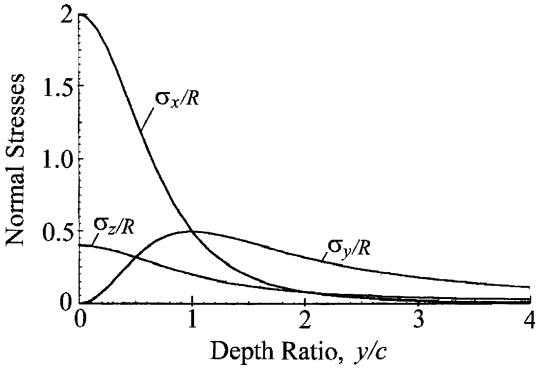

Fig. 3. Normal stresses as a function of depth for the spalling model, on the plane of symmetry $x = 0$. The shear stress is zero on this plane.

4. Subsurface explosive cracking

The second mode of lightning-induced failure is that thermal shock leads to the sudden expansion of water entrained in the solid's pore cavities, an expansion that can lead to explosive crack propagation from those cavities. In the fracture analysis that follows, the previous spalling model consisting of a two-dimensional hydrostatic strip (Fig. 2) is abandoned. Now this strip is assumed to have the same properties as the whole solid, including pore cavities. In Portland cement concrete and in gravel concrete building block, such cavities are about 0.5 μm in diameter; and the total water can be as high as 10% by volume (Cordon, 1979). The size of water-containing pore cavities in naturally occurring rocks is from 1 to 5 μm long and the pore water content as a percent of dry weight varies from 0.01% for diabase, to 0.1% for granite, and to 5% for dolomite (Deere and Miller, 1966).

4.1. Fracture mechanics

An idealized model of a single, water-filled pore cavity embedded within a solid, either concrete or natural rock, is shown in Fig. 4a. This pore cavity is assumed to be penny-shaped of radius a, and oriented with its face parallel to the plane $x = 0$. This particular type of cavity geometry was chosen because $\mathscr{K}_\sigma$, the crack tip stress intensity factor, is known. It is noted that ellipsoidal and spherical cavities were not chosen for study because explicit forms for $\mathscr{K}_\sigma$ have yet to be computed for those geometries. In reality, there are numerous pore cavities of various shapes and at different orientations. As a further idealization, it is assumed that the material surrounding the single penny-shaped cavity is linearly elastic, with homogeneous and isotropic properties. With these assumptions, the critical pore pressure p_c that leads to the radial propagation of cracks from this pore cavity can be computed. The following results are based on modern fracture mechanics and on the compiled works of Tada et al. (2000).

Radial cracking of the penny-shaped cavity can take place for two types of loading. The first type of loading, shown in Fig. 4b, is a far-field uniform stress σ, which is normal to the cavity face. The mode I crack-tip stress intensity factor for this loading is

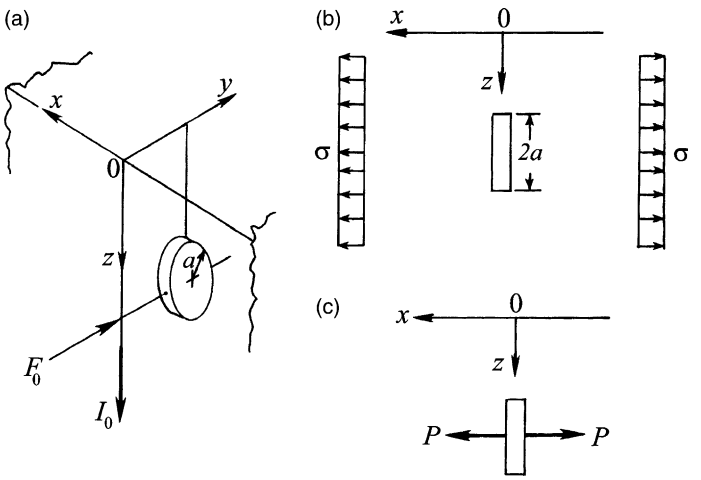

Fig. 4. Internal crack model showing (a) orientation of the penny-shaped, water-filled cavity, (b) cavity subjected to a far-field uniform stress and (c) the cavity subjected to opposing central wall loads.

$$\mathscr{K}_\sigma = \frac{2}{\pi}\sigma\sqrt{\pi a} \tag{20}$$

The second type of loading, shown in Fig. 4c, is the opposing pair of central loads P normal to the cavity walls, for which the mode I crack-tip stress intensity factor is

$$\mathscr{K}_P = \frac{P}{(\pi a)^{3/2}} = \sqrt{\frac{a}{\pi}}p_c \tag{21}$$

In the last equation, the load P was replaced by the statically equivalent load due to the critical cavity water pressure p_c, or $P = \pi a^2 p_c$. For the radial crack to propagate, define σ_t as the tensile strength of the solid and let $\mathscr{K}_\sigma = \mathscr{K}_P$. The result for the critical cavity pressure is thus

$$p_c = 2\sigma_t \tag{22}$$

which is independent of the pore cavity radius a and cavity orientation.

It is further noted that a critical cavity pore pressure of twice that of the tensile strength is necessary to propagate this penny-shaped crack, whereas the pressure required to propagate an elliptical crack that passes entirely through a flat plate is smaller, or $p_c = 1.57\sigma_t$. See Tada et al. (2000) and Wilson (1977). It is logical that the more embedded and more constrained penny-shaped pore cavity should require the higher critical pressure.

4.2. Pressure–temperature behavior

Consider a lower bound on the temperature change T required to raise the cavity pore pressure to a critical value p_c. To do this, assume that the water pressure in a cavity pore is initially at atmospheric pressure ($p = 0$) at $T = 0$ °C. Also assume that the specific volume $v = 10^{-3}$ m^3/kg of pore cavity water remains fixed as T is increased; that is, a fixed mass of water in a rigid container is subjected to an increasing temperature. This T vs. p relationship is shown in the lower curve of Fig. 5, which is based on data in

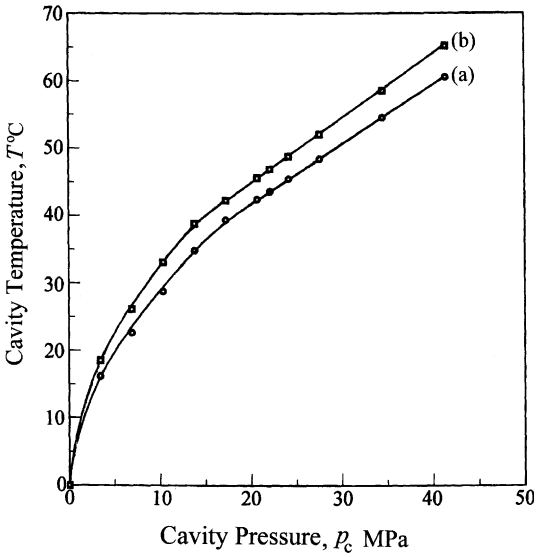

Fig. 5. Pressure–temperature behavior for a fixed mass of water: (a) water confined in a rigid cavity (fixed volume) and (b) water confined to a cavity in a concrete block that expands freely with increasing temperature, where $\alpha_0 = 10.3 \times 10^{-6}$ °C^{-1}.

Keenan et al. (1969). For example, for a solid with a tensile strength of $\sigma_t = 10.34$ MPa, the critical pressure for a crack to propagate is $p_c = 20.68$ MPa, from Eq. (22), and the corresponding minimum temperature increase is 42.4 °C. As shown next, this temperature would be higher if the effect of the solid volume expansion with a rise in temperature were included.

An upper bound on the temperature required to produce p_c can be deduced as follows. Assume that a volume of the solid that surrounds the penny-shaped crack expands freely under a uniform temperature increase T. For this stress-free volume, the principal strains are due to temperature only, or

$$\varepsilon_x = \varepsilon_y = \varepsilon_z = \alpha_0 T \tag{23}$$

Define Δ as the *dilatation*, or the increment in this volume per unit volume. For small strains, Love (1944) showed that Δ is equal to the sum of the principal strains, which leads to

$$\Delta = 3\alpha_0 T \tag{24}$$

With this result and a nominal value of $\alpha_0 = 10.8 \times 10^{-6}$ °C^{-1} for concrete block, together with the measured properties of water (Keenan et al., 1969), the upper bound curve of T vs. p shown in Fig. 5 was deduced. Here, the specific volume v of the pore cavity water at $T = 0$ °C, or $v = 10^{-3}$ m^3/kg, was multiplied by $(1 + \Delta)$ and a compatible set (v, p, T) was computed by trial and success and data interpolation. Unlike the lower bound curve, this upper bound curve depends on the coefficient of linear expansion α_0 of the solid. It is noted that the temperature gap between the upper and lower bound curves at constant pressure increases or decreases as α_0 increases or decreases, respectively. For the example shown in Fig. 5, this temperature gap is in the range of 4–5 °C for most of the range of pore cavity pressure.

Realistically, there are confining compressive stresses surrounding the unit volume containing the pore cavity—stresses that reduce the value of Δ given by Eq. (24) and consequently reduce the value of T required to produce the cavity pressure p. Thus, just prior to crack propagation, the actual T vs. p behavior is a curve that lies somewhere between the two curves shown in Fig. 5.

5. Case studies and discussion

The two case studies that follow involve a concrete building block (Case A) and a sandstone monument (Case B). Their thermal and mechanical properties are listed in Table 2. Other material characteristics that are not explicit in the final analyses, but are implicit in the physical models, are the geometry and abundance of the water filled cavities. For concrete blocks commonly used in building construction, the capillary cavities containing water average about 0.5 μm in diameter and the total water content is about 10% by volume (Cordon, 1979). For a typical sandstone, water is contained in the interparticle pore spaces, which

Table 2
Properties of materials for two case studies (Cordon, 1979; Deere and Miller, 1966; McAdams, 1954)

	Property	Case A concrete block (Gravel aggregate)	Case B sandstone (Berea)
c_p	Specific heat (J °C^{-1}/kg)	837	698
k	Thermal conductivity (W °C^{-1}/m)	1.86	1.83
α	Thermal diffusivity (m^2/s)	1.01×10^{-6}	1.17×10^{-6}
γ	Density (kg/m^3)	2200	2240
E	Young's modulus (GPa)	24.1	23.6
α_0	Coefficient of linear expansion (°C^{-1})	10.8×10^{-6}	9.36×10^{-6}
σ_c	Compressive strength (MPa)	29.6	73.8
σ_t	Tensile strength (MPa)	3.45	1.17
ν	Poisson's ratio	0.2	0.08–0.40

are about 5 μm in length, and in the capillary cavities, which are 1–2 μm in length. Berea sandstone, the material assumed for Case B, contains about 2% water by volume (Deere and Miller, 1966). Thus, these two materials are candidates for fracture by lightning.

5.1. Case A

In an experiment documented on videotape, an upright, ungrounded concrete block was struck by a laboratory spark to simulate lightning (Aiello, 1997). Shown in Fig. 6 are representations of two consecutive video images of this experiment, where the time between the two images was 0.033 s. In the first image, Fig. 6a, the plasma is travelling down the block and has begun to disperse, and block fracture is impending. In the second image, Fig. 6b, the plasma has impacted the floor and is dispersing, and the nearly vertical fracture of the block is complete. The video images indicate that the block was exposed to the plasma for approximately $\Delta t = 0.1$ s. Close examination of the images (permission to reproduce them was denied) showed a clean separation without spalling for most of the height of the block. Near and at the base of the block, however, there was evidence of some spalling surrounding the fracture line. These observations are consistent with the more severe base spalling observed for a partially buried foundation wall which acted as a conduit for lightning on its way to ground (Wilson, 1977, 2000).

The following partial data were available on the characteristics of this laboratory spark experiment: a spark path length of $d = 6$ m, and a potential from the current source to ground of $V = 3 \times 10^6$ V. The following reasonable estimates are made for the unknown data in this experiment: a core current of $I_0 = 15$ A, and values for two parameters based on lightning leaders (Table 1): $c = 6.6$ cm and $f_r = 0.01$. With these additional data and with an assumed value $f_s = 0.25$, an estimate of the flux F_0 to which the block was exposed just prior to the time that the plasma impacted the base, was computed from Eq. (4) as $F_0 = 142$ kW/m^2.

It is now shown that the two mathematical models previously developed do complement the experimental results. Refer to the coordinate system defined in Figs. 1 and 4, in which the impending crack occurs adjacent to the plasma core on the plane $x = 0$. First, compute the temperature change T in the block adjacent to the plasma during its 0.1 s strike. Given $F_0 = 142$ kW/m^2 and the thermal properties of k and α in Table 2, an upper bound for the temperature variation with depth y of the impending crack was com-

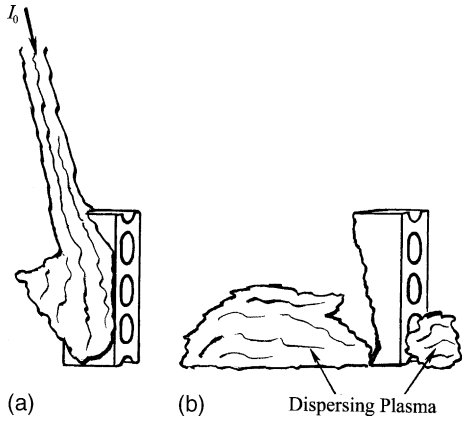

Fig. 6. Representations of consecutive video frames for the Case A experiment in which a laboratory spark strikes an ungrounded gravel concrete building block: (a) the channel spark and block just prior to fracture and (b) the fractured block at a time 0.033 s later, showing some spalling at the base and the dispersing plasma.

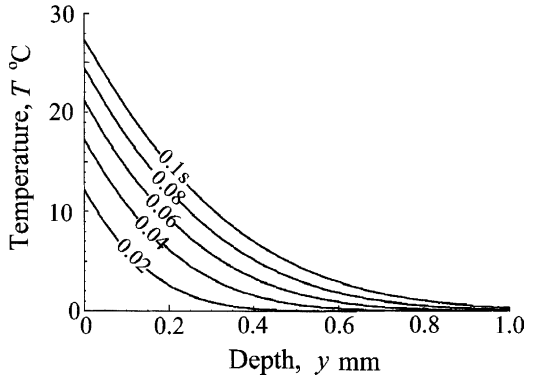

Fig. 7. Case A: a simulation of the experiment. Snapshot views show the predicted temperature distributions with depth on the plane $x = 0$, for several times up to the total flash time of $\Delta t = 0.1$ s. The heat flux is $F_0 = 142$ kW/m^2.

puted from Eq. (7). The results are shown in Fig. 7 as snapshot views of T vs. y for several times up to the 0.1 s duration of the flash.

Shown in Table 3 are the computed parameters for Case A. The observations and conclusions based on these results are summarized as follows.

- At the end of the flash of duration of 0.1 s, the temperature change in the block varied from 27 °C at the surface $y = 0$ to nearly zero at $y = 1$ mm. Thus $h = 1$ mm was chosen as the strip thickness.
- The critical temperature for spalling was $T_t = 550$ °C, which is well above the mean strip temperature of $\overline{T} = 10$ °C at the end of the flash. This is consistent with observations that showed no evidence of spalling along the line of fracture, for most of the height of the block.
- The slight spalling observed at the base of the concrete block can be explained. There was a momentary "pileup" of plasma energy as the current stream came to an abrupt halt and began to disperse at the floor. At this moment, it is reasonable that sufficient plasma energy was radiated to the block's base to raise the local mean strip temperature above the critical spalling temperature of $\overline{T}_t = 550$ °C. To achieve this elevated temperature, the momentary base flux level needed to be 55 times the steady value of 142 kW/m^2, or $F_0 = 7810$ kW/m^2. Since the temperature of the current-carrying cores of lightning leaders is nominally about 2700 °C near ground (Table 1), it is hypothesized that such temperatures could have been achieved in the experimental simulation as well, thus leading to the elevated local flux and spalling at the base.

Table 3
Computed results for the two case studies

	Parameter	Case A	Case B
h	Strip depth (mm): Figs. 7,8	1.0	2.0
p_c	Critical cavity pressure (MPa): Eq. (22)	6.90	2.34
F_0	Heat flux (kW/m^2)	142	60.6
R	Radiant heat parameter (MPa): Eq. (17)	0.125	0.0729
σ_x(max)	Peak stress (MPa): Fig. 3	0.250	0.146
T	Temperature of solid at $x = 0$ (°C): Eq. (7)	0–27	0–28.5
$\overline{T}$	Mean strip temperature (°C): Figs. 7,8	10	13
T_t	Critical temperature for spalling (°C): Eq. (19)	550	104
T_c	Critical cavity temperature (°C): Fig. 5	24–29	13–15

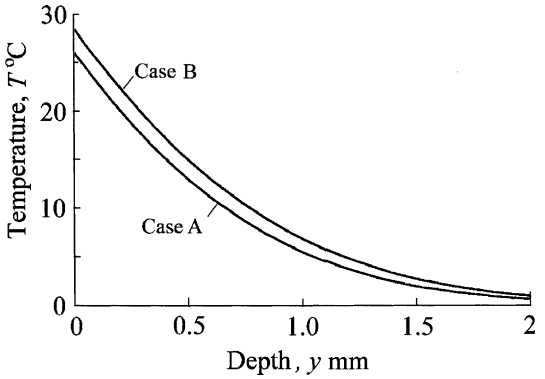

Fig. 8. Cases A and B: predicted temperature distributions with depth on the plane $x = 0$, based on a nominal lightning leader with a heat flux of $F_0 = 60.6$ kW/m^2 and a total flash time of $\Delta t = 0.5$ s.

- The important conclusion of this case study is that explosive, subsurface cracking was the primary cause of block failure. For this to occur, the critical cavity water pore pressure was $p_c = 2\sigma_t = 6.90$ MPa, which can be achieved in this solid for temperature changes between 24 and 29 °C (Fig. 5). At the end of the flash, the predicted near-surface block temperatures were within this range (Fig. 7).
- It appears that this experiment was a good simulation of lightning leaders. To show this, suppose that an identical block were struck by a lightning leader with a nominal flux of $F_0 = 60.6$ kW/m^2 and a flash time of $\Delta t = 0.5$ s. Based on the same analysis and material properties used for the experimental block, the temperature distribution at $y = 0$ for the identical block was computed. The results are shown in Fig. 8, which indicate that there are near-surface temperatures in the same critical range as those for the experimental case: 24–29 °C. Thus, if an identical block were struck by a lightning leader, damage similar to that observed in Fig. 6b could be expected.

5.2. Case B

The Ring of Brodgar is an impressive circle of upright sandstones located in the Orkney Islands, UK. Of the original 60 stones, which were erected about 2500 BC, only 27 remain standing at this time. The ring is 103.7 m in diameter and the height of the remaining stones varies from 2 to 4.6 m. A photograph of a fallen stone is shown in Fig. 9, for which the following sign is posted.

Visitor information

This stone was struck by lightning on June 5th 1980 causing it to shatter. Such events may also have occurred in earlier times, and might account for the damaged state of several other stones in the ring.

This toppled stone has a split along its longitudinal axis, along which the lightning leader probably traveled to ground. Spalling near and at the base is apparent, and this together with the longitudinal cracking sufficiently undermined this monument, causing it to topple.

The quantitative models for spalling and internal explosive cracking were applied to this event and the results are listed in Table 3. Those results are based on the nominal properties of lightning leaders listed in Table 1, which led to the nominal heat flux of $F_0 = 60.6$ kW/m^2. Other chosen parameters were: $c = 6.6$ cm, $f_s = 0.25$, and $\Delta t = 0.5$ s. Further, the material properties for the monument are assumed to closely

Fig. 9. This is a photograph of a sandstone monument that toppled when it was struck by lightning in 1980. Spalling is observed at its base, at the right of the photograph; and the deep midwidth fracture extends the full 4 m length of this stone. A partial view of one of the remaining 27 upright stones in this historic Ring of Brodgar, located in the Orkney Islands, UK, is observed in the upper left corner of the photograph.

resemble those of Berea sandstone, properties for which are listed in Table 2. The observations and conclusions for this case are summarized as follows.

- At the end of the flash of duration 0.5 s, the temperature of the sandstone adjacent to the current core varied from 28.5 °C at the surface $y = 0$ to nearly zero at $y = 2$ mm. See the upper curve of Fig. 8. Thus, $h = 2$ mm was chosen as the strip thickness.
- The critical temperature for spalling is 104 °C, which is well above the mean strip temperature of $\overline{T} =$ 13 °C.
- As for Case A and for the previous cases investigated (Wilson, 1977, 2000), the spalling observed near and at the base was probably due to plasma "pileup" as the lightning leader's current stream came to an abrupt halt at ground. Thus, the concentration of the near-base flux was at least $F_0 = (104/13)(60.6) =$ 485 kW/m^2.
- As for Case A, explosive subsurface cracking was the primary cause for the longitudinal crack. For cracking, the critical water pore pressure was $p_c = 2.34$ MPa, which can be achieved for the sandstone for a temperature change in the range of 13–15 °C (Fig. 5).
- At the end of the flash, the predicted temperature change adjacent to the current core exceeded 15 °C for depths of up to 0.4 mm (Fig. 8). The depth of 0.4 mm corresponds to 80–400 cavity lengths in the sandstone.

6. Conclusions

The present investigation introduces two general analytical models to explain the failure modes of free-standing masonry and rock structures subjected to lightning strikes. The following conclusions are based on these models, complemented with experimental data of two case studies.

- For failure by the first mode, spalling, the predicted lightning-induced temperature changes (thermal shocks) for a common masonry block (Case A) and for a sandstone monument (Case B) were at least 550 and 100 °C, respectively.
- Experimental evidence indicates that spalling occurs at the end of the strike and only in the proximity of the base of these solids, where the lightning-generated heat flux is momentarily of particularly high concentration.
- For failure by the second mode, explosive subsurface fracture of water-filled cavities, the predicted lightning-induced temperature changes for the masonry block and the sandstone monument were at least 24 and 13 °C, respectively.
- Experimental evidence indicates that explosive subsurface fracture occurs for the whole duration of the strike as the lightning leader's plasma core propagates to ground along a vertical surface of the solid.
- Experimental measures are needed for the surface and subsurface temperatures of solids as they are struck by lightning. Such measurements will help to validate the two hypothesized failure modes proposed in the present investigation.

Acknowledgements

The author thanks Ronald S. Perkins of Duke University for sharing data on the properties of rocks and also thanks the reviewers for their helpful comments.

References

Aiello, R., 1997. Raging planet lightning (video). Discovery Communications, Inc., Bethesda, MD.

Bazant, Z.P., Kaplan, M.F., 1996. Concrete at High Temperatures. Longman–Addison-Wesley, London.

Carslaw, J.H., Jaegar, J.C., 1990. Conduction of Heat in Solids, second ed. Oxford Press, UK.

Cordon, W.A., 1979. Properties, Evaluation, and Control of Engineering Materials. McGraw-Hill Book Company, Inc., New York.

D'Alessandro, F., Gumley, J.R., 2001. A collection volume method for the placement of air terminals for the protection of structures against lightning. Journal of Electrostatics 50, 279–302.

Deere, D.U., Miller, R.P., 1966. Engineering Classification and Index Properties for Intact Rock. AD 646610, US Department of Commerce, Washington, DC.

Frydenlund, M.M., 1986. Controlling lightning's wrath. Rural Living 4, 10–16. Lightning Protection Institute, Harvard, IL.

Keenan, J.H., Keyes, F.G., Hill, P.G., Moore, J.G., 1969. Steam Tables: Thermodynamic Properties of Water including Vapor, liquid, and Solid Phases. John Wiley and Sons, Inc., New York.

Krider, E.P., 1982. A review of natural lightning: experimental data and modeling. IEEE Transactions on Electromagnetic Compatibility 24 (2), 79–112.

Love, A.E.H., 1944. A Treatise on the Mathematical Theory of Elasticity, fourth ed. Dover Publications, New York.

McAdams, W.H., 1954. Heat Transmision. McGraw-Hill Book Company, Inc., New York.

Michell, J.H., 1900. Proceedings of the London Mathematical Society, vol. 32, pp. 35–44.

Orville, R.E., Uman, M.A., Sletten, A.M., 1967. Temperature and electron density in long sparks. Journal of Applied Physics 38, 895–896.

Petrov, N.I., D'Alessandro, F., 2002. Assessment of protection system positioning and models using observations of lightning strikes to structures. Proceedings of the Royal Society of London A 458, 723–742.

Sadowsky, M.A., 1955. Thermal shock on a circular surface of exposure of an elastic half space. Journal of Applied Mechanics 22, 177–182.

Tada, H., Paris, P.C., Irwin, G.R., 2000. The Stress Analysis of Cracks Handbook, third ed. ASME Press, New York.

Timoshenko, S., Goodier, J.N., 1951. Theory of Elasticity, second ed. McGraw-Hill Book Company, Inc., New York.

Uman, M.A., 1984. Lightning. Dover Publications, Inc., New York.

Wilson, J.F., 1977. Lightning damage to masonry structures. Journal of Products Liability 1 (4), 237–250.

Wilson, J.F., 2000. Forensic engineering data showing lightning damage to structures. Journal of the National Academy of Forensic Engineers 17 (2), 41–54.